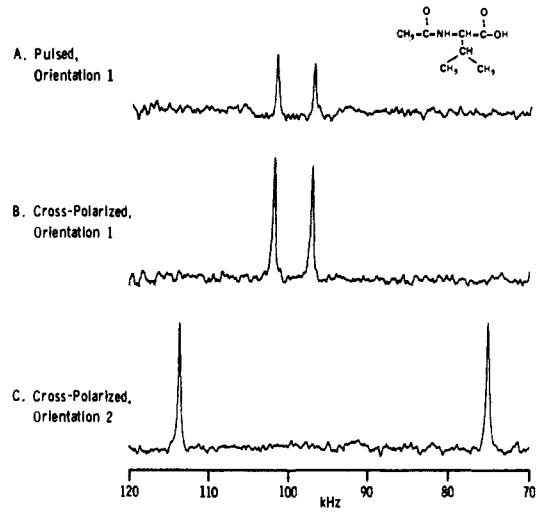

Figure 2. Proton-decoupled ^{14}N overtone NMR spectra of a single crystal of *N*-acetylvaline. (A) Directly pulsed spectrum, using a 30-ms nitrogen overtone if pulse at 36.212 MHz (ν_0 = 18.059 MHz); 1024 transients with a 1-s recycle delay. The two lines arise from two inequivalent molecules in the unit cell. The frequency scale is relative to $2\nu_0$ = 36.118 MHz. (B) Spectrum obtained with cross-polarization from proton dipolar order, demonstrating signal enhancement 1024 transients with a 1-s recycle delay. (C) Spectrum obtained with cross-polarization after an arbitrary 10° rotation of the crystal, illustrating the sensitivity of the overtone frequencies to orientation.

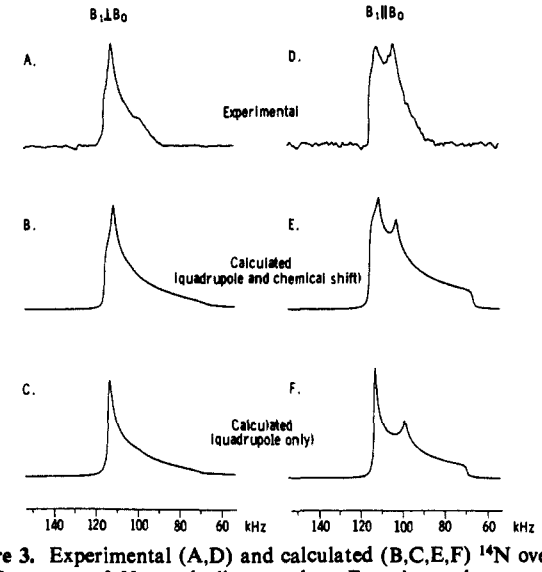

Figure 3. Experimental (A,D) and calculated (B,C,E,F) ^{14}N overtone NMR spectra of *N*-acetylvaline powder. Experimental spectra were obtained with proton decoupling and cross-polarization. The overtone if field B_1 was applied perpendicular to the static field B_0 in (A)–(C) and parallel to B_0 in (D)–(F). Each experimental spectrum is the result of approximately 30 000 scans with a carrier frequency of 36.225 MHz. In the calculated spectra, the signal contribution of each crystallite orientation is weighted by the magnitude of the overtone transition moment at that orientation. In the experimental spectra, the intensities are determined by both the transition moment and the cross-polarization efficiency. Both second-order quadrupole shifts and chemical shifts were included in the calculations of (B) and (E); only second-order quadrupole shifts were considered in the calculations of (C) and (F).

Jeener–Broekaert sequence.[28] Figure 2C illustrates the sensitivity of the overtone frequencies to molecular orientation, primarily due to the orientational dependence of $\nu_Q^{(2)}$.

Figure 3 contains the first overtone NMR spectra of a polycrystalline sample. Spectra of a 230-mg powder sample of *N*-acetylvaline were obtained with two different double-resonance probe configurations. The spectrum in Figure 3A was obtained by using a double-tuned probe with a radiofrequency solenoid coil perpendicular to the static field B_0, which is the usual configuration in solid-state NMR. The spectrum in Figure 3D was obtained by using a probe with a solenoid coil *parallel to* B_0[1,29] for ^{14}N irradiation near $2\nu_0$ and a Helmholtz coil perpendicular to B_0 for proton irradiation. The fact that two sharp features appear in Figure 3D while only a single sharp feature appears in Figure 3A is a consequence of the different orientational dependences of the overtone transition moment in the two coil configurations.

The positions of the sharp features in Figure 3A,D are determined primarily by the values of e^2qQ/h and the quadrupole asymmetry parameter η. In addition, effects of chemical shift anisotropy (CSA) are apparent in the details of the shapes of the spectral features. Parts B and E of Figure 3 are calculated overtone powder patterns for the perpendicular and parallel coil configurations in which the values e^2qQ/h = 3.24 MHz and η = 0.27 were used, along with an axially symmetric CSA tensor characterized by $\sigma_\parallel = -114$ ppm and $\sigma_\perp = 57$ ppm. The values of e^2qQ/h and η were determined from the experimental spectra, and are in good agreement with previously reported values.[8,30] The values of $\sigma_\parallel$ and $\sigma_\perp$ were taken from ^{15}N NMR studies of peptides and proteins.[31,32] In Figure 3B,E the principal axis of the CSA tensor was taken to be aligned with the x axis of the quadrupole tensor. Parts C and F of Figure 3 are powder patterns calculated without including CSA effects, showing that the quadrupole interaction accounts for the principal features of the experimental spectra.

Acknowledgment. We thank M. Bloom for communicating his results prior to publication and P. Stewart for the loan of the *N*-acetylvaline crystal. This research was supported in parts by grants (GM-24266 and GM-29754) from the N.I.H. R.T. acknowledges support from a Damon Runyon–Walter Winchell Cancer Fund Fellowship, DRG-891.

Registry No. *N*-Acetylvaline, 96-81-1.

(28) Jeener, J.; Broekaert, P. *Phys. Rev.* **1967**, *157*, 232–240.

(29) (a) Analogous effects have been exploited in EPR studies of optically excited triplet states. (b) van der Waals, J. H.; de Groot, M. S. *Mol. Phys.* **1959**, *2*, 333–340. (c) de Groot, M. S.; van der Waals, J. H. *Mol. Phys.* **1960**, *3*, 190–200.

(30) Sadiq, G. F.; Greenbaum, S. G.; Bray, P. J. *Org. Magn. Reson.* **1981**, *17*, 191–193.

(31) Harbison, G. S.; Jelinski, L. W.; Stark, R. E.; Torchia, D. A.; Herzfeld, J.; Griffin, R. G. *J. Magn. Reson.* **1984**, *60*, 79–82.

(32) Cross, T. A.; Opella, S. J. *J. Mol. Biol.* **1985**, *182*, 367–381.

Catalytic Decomposition of 2-Propanol on Single-Crystal Surfaces of ZnO

P. Berlowitz and H. H. Kung*

Chemical Engineering Department and the Ipatieff Laboratory, Northwestern University Evanston, Illinois 60201

Received December 30, 1985

The concept of Bourdart[1] of structure sensitivity in heterogeneous catalytic reactions suggests that the kinetics and the mechanism of a reaction may depend on the surface structure and the crystalline size of the catalyst. Investigation of the surface structural effect is made possible by surface science techniques using single-crystal samples.[2-4] It is interesting to note that all the examples reported have been on metal surfaces. We report here the first example of surface structural effect on single-crystal surfaces of an oxide, specifically zinc oxide.

(1) Boudart, M. *Adv. Catal.* **1969**, *20*, 153.

(2) Blakely, D. W.; Somorjai, G. A. *J. Catal.* **1976**, *42*, 181.

(3) Gale, G. J.; Salmeron, M.; Somorjai, G. A. *Phys. Rev. Lett.* **1977**, *38*, 1027; *J. Chem. Phys.* **1977**, *67*, 5324.

(4) Somorjai, G. A. *Chemistry in Two Dimensions, Surfaces*, Cornell University Press: New York, 1981.

0002-7863/86/1508-3532$01.50/0

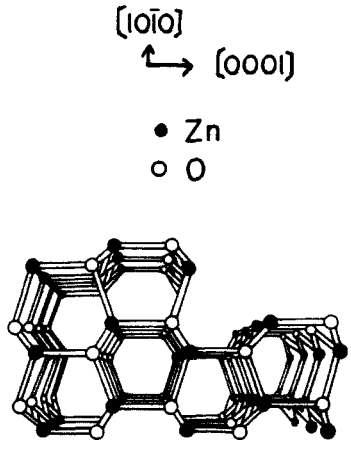

Figure 1. Schematic drawing showing the atomic arrangement of different ZnO surfaces. The right vertical surface is the Zn-polar face, the left vertical surface is the O-polar face, and the top surface is the stepped nonpolar face.

The existence of surface structural effects on oxides can be inferred from results of catalytic studies using powder polycrystalline samples. This has been particularly well documented on molybdenum oxide catalysts for oxidation reactions.[5,6] Similar effects have also been reported on vanadium oxide catalysts.[7-9] On zinc oxide, these effects have been demonstrated by using single-crystal surfaces in the temperature-programmed decomposition of methanol, 2-propanol, formaldehyde, and formic acid,[10-12] as well as on polycrystalline samples.[13] In general, the fraction of adsorbate decomposed and the temperature of decomposition are the highest on the zinc-polar (0001) surface, intermediate on the stepped nonpolar (50$\bar{5}$1) surface, and the lowest on the oxygen-polar (000$\bar{1}$) surface. (A schematic representation of these surfaces is shown in Figure 1.) These studies, however, were noncatalytic. Here we report the results of the catalytic decomposition of 2-propanol on these ZnO surfaces.

The catalytic reaction was conducted in the ultrahigh-vacuum chamber described before.[10,11] The system was equipped with a low-energy electron diffractometer, an Auger electron spectrometer, and a quadrupole mass spectrometer. The zinc oxide single-crystal surfaces were prepared in the same manner as previously described.[10,11] They were heated by being in contact with a tantalum foil that was resistively heated with electrical current.[14] 2-Propanol was introduced directly at the surface being studied by a stainless steel needle, which was at an angle of about 40° with the surface normal.[15] Such an arrangement was similar to the one used by Yates and co-workers.[16] Reactions due to the side or the back of the crystal were minimized by coating these parts of the crystal with evaporated gold.

The flux of 2-propanol onto the surface was calculated by monitoring the pressure drop of the feed line of a known volume and from the known geometry of the system. 2-Propanol was assumed to leave the needle in an effusive flux. It was estimated that a point-to-point variation of the flux of 5-fold was present over the crystal surface. From the flux, an average effective pressure of 2-propanol was calculated. Experiments were performed over an effective pressure up to 4 mtorr. The pressure dependence of reaction rate was determined for the Zn-polar surface at 235 °C and the stepped (50$\bar{5}$1) surface at 335 °C. Between 0.14 to 2.5 mtorr, the rate of decomposition of 2-propanol increased linearly with pressure. That is, the reaction was first order in 2-propanol pressure. Normally, an experiment had to be stopped after 60–90 min because of the buildup of the H_2 background pressure. Assuming that every surface Zn–O pair was equivalent and catalytically active, the time corresponded to one to five turnovers per Zn–O pair. Experiments were continued on the same crystal after pumping down the chamber and flashing the crystal to 500 °C for 2 min. AES analyses of the crystals after one experiment did not show significant carbon buildup or other impurities. The crystal was usually cleaned by sputtering after three to five experiments.

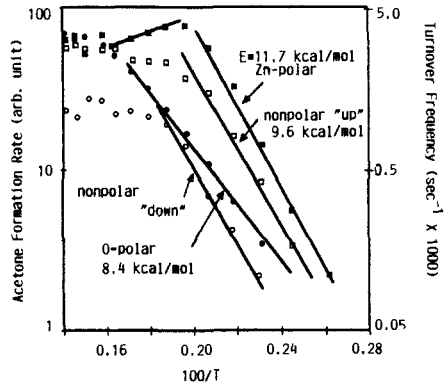

Figure 2. Temperature dependence of the rate of acetone production on different ZnO surfaces. "Up" and "down" stand for molecules approaching the nonpolar stepped surfaces in the direction up-the-step and down-the-step, respectively.

Dehydrogenation of 2-propanol to acetone was the major decomposition pathway on all surfaces, accounting for over 90% of the reaction. The minor pathway was the dehydration to propene. Owing to the large relative uncertainties in the small propene and water signals from the mass spectrometer, the selectivities were determined to no better than 5%. Within this uncertainty, there did not seem to be any variations in the selectivity on different crystal surfaces.

The temperature variation of the reaction rate was determined for the different surfaces from 110 to 435 °C. The rates at an average effective pressure of 0.71 mtorr are shown in Figure 2, which also shows the turnover frequencies calculated by using the geometric surface area. After correcting for the pressure difference, the turnover frequencies are within a factor of 2–10 to that reported by Davignon et al. on ZnO powder samples.[19] On all the surfaces studied, the rates increased with increasing temperature up to about 260 °C when the rates either decreased with further increase in temperature or remained roughly constant, which is commonly observed in low-pressure reaction studies.[17,18] In the high-temperature region, the observed rate decreases because the decrease in the surface coverage with increasing temperature due to lowering of the equilibrium surface coverage and/or decrease in the sticking coefficient of the reactant is faster than the increase in the reaction rate constant. The rates were the highest on the Zn-polar surface, which were about 3–5 times higher than on the O-polar surface. For the nonpolar stepped surface, the rates depended on the direction of approach of the reactant molecules. They were 3–4 times higher if the molecules approached along the direction up-the-steps than if they ap-

(5) Volta, J. C.; Portefaix, J. L. *Appl. Catal.* **1985**, *18*, 1.
(6) Tatibouet, J. M.; Germain, J. E.; Volta, J. C. *J. Catal.* **1983**, *82*, 240. Volta, J. C.; Tatibouet, J. M. *J. Catal.* **1985**, *93*, 467.
(7) Mori, K.; Miura, M.; Miyamoto, A.; Murakami, Y. *J. Phys. Chem.* **1984**, *88*, 5232.
(8) Mori, K.; Miyamoto, A.; Murakami, Y. *J. Phys. Chem.* **1984**, *88*, 2735; **1984**, *88*, 2741.
(9) Kung, H. H.; Kung, M. C. *Adv. Catal.* **1985**, *33*, 159.
(10) Akhter, S.; Lui, K.; Kung, H. H. *J. Phys. Chem.* **1985**, *89*, 1958.
(11) Cheng, W. H.; Akhter, S.; Kung, H. H. *J. Catal.* **1983**, *82*, 341.
(12) Lui, K.; Akhter, S.; Kung, H. H. *Solid State Chemistry in Catalysis*; Grasselli, R. K., Brazdil, J. F., Eds.; ACS Symp. Ser. 279; American Chemical Society: Washington, DC, 1985; p 205.
(13) Bowker, M.; Houghton, H.; Waugh, K. C.; Giddings, T.; Green, M. *J. Catal.* **1983**, *84*, 252.
(14) Lui, K.; Vest, M.; Akhter, S.; Berlowitz, P.; Kung, H. H. *J. Phys. Chem.*, in press.
(15) Berlowitz, P. Ph.D. Thesis, Northwestern University, Evanton, IL, 1985.
(16) Gates, S. M.; Russel, J. N., Jr.; Yates, J. *J. Catal.* **1985**, *92*, 25.
(17) Bonzel, H. P.; Ku, R. *J. Vac. Sci. Technol.* **1972**, *9*, 663.
(18) Engel, T.; Ertl, G.; *J. Chem. Phys.* **1978**, *69*, 1267; *Adv. Catal.* **1979**, *28*, 1.
(19) Djega-Mariadassou, G.; Davignon, L. *J. Chem. Soc., Faraday Trans. 1* **1982**, *78*, 2447.

proached down-the-steps. A similar observation has also been reported for the H_2–D_2 exchange reaction on platinum surfaces.[3]

The rates below 260 °C followed the Arrhenius behavior. The activation energy for this region was 11.7 ± 1.0 kcal/mol for the Zn-polar surface, 9.7 ± 1.0 kcal/mol for the nonpolar stepped surface, and 8.4 ± 1.0 kcal/mol for the O-polar surface. It should be noted that the activation energy for the stepped surface did not depend on the direction of approach, unlike the rates. Thus the enhanced rate in the "up" direction of approach must be due to a higher sticking coefficient of reactants in that direction, while the surface reaction probability remains the same.

The trends in the activation energy and the reaction rates follow those derived from temperature-programmed decomposition studies.[11,12] This trend has been explained by the different magnitudes of surface dipole, different hardness of the surface Zn ions, and different degrees of steric hindrance by the surrounding oxygen ions to the interaction of adsorbates with surface Zn ions on the different surfaces. It appears that these factors can be used to explain the trends in catalytic reactions as well.

Acknowledgment. Acknowledgment is made to the donors of the Petroleum Research Fund, administered by the American Chemical Society.

First Electride Crystal Structure

Steven B. Dawes, Donald L. Ward, Rui He Huang, and James L. Dye*

Department of Chemistry, Michigan State University East Lansing, Michigan 48824

Received January 21, 1986

The crystal structure and optical, electrical, and magnetic properties of $Cs^+(18C6)_2 \cdot e^-$ (18C6 = 18-crown-6) show that each electron is trapped in a nearly spherical, otherwise empty, cavity of radius ~2.4 Å, surrounded by eight sandwich-complexed cesium cations. The shortest interelectron distance (8.68 Å) results in only weak coupling, so that this salt behaves as a localized electride.

When the first salt of an alkali metal anion was synthesized in 1974,[1,2] "blue, strongly paramagnetic solids" were also obtained by evaporation of ethylamine solutions that contained cryptated cations and solvated electrons.[2] This method permitted observation of the optical spectrum of a solvent-free electride[3] and led to intensive efforts to isolate crystalline electrides. Rapid autocatalytic decomposition of solutions frustrated these attempts until 1983, when crystals of the subject electride, $Cs^+(18C6)_2 \cdot e^-$, were isolated.[4,5]

Eight crystalline electrides have now been synthesized. The optical, electrical, and magnetic properties range from those of weakly interacting localized electrons,[4,6] to antiferromagnetism[7] and spin-paired states,[8,9] to electron delocalization.[9,10] This variability makes the nature of electron trapping in electrides a subject of great interest.

The electride, $Cs^+(18C6)_2 \cdot e^-$, crystallizes from dimethyl ether–trimethylamine mixtures as shiny black plates. The optical transmission spectrum of thin films consists of a single broad band with maximum absorbance at 1650 nm.[4] The low absorbance at wavelengths greater than 2000 nm indicates electron localization with a trap depth of at least 0.5 eV. The conductivity is consistent with electron localization since it shows semiconductor-like behavior with a band gap of 0.9 eV.[4,5]

Magnetic susceptibilities, down to ~2 K, nearly obey the Curie–Weiss law.[6] A single narrow EPR line (0.5 G down to 2 K) occurs at the free electron g value. The ^{133}Cs NMR spectrum of the solid exhibits a temperature-dependent chemical shift that corresponds to only 0.033% atomic character.[11] Thus, this electride has all of the characteristics expected of a compound in which all of the electrons are trapped at anion vacancies. This view is further strengthened by NMR evidence that up to three electrons around Cs^+ can be replaced by Na^- ions.[11] Since the crystal structure of $Cs^+(18C6)_2 \cdot Na^-$ shows that there are eight Na^- ions around each sandwiched cesium cation,[12] it seemed likely that the electride structure is similar to that of the sodide, with electrons occupying *all* of the anionic sites.

The crystal structure of $Cs^+(18C6)_2 \cdot e^-$ [$CsC_{24}H_{48}O_{12}$] was

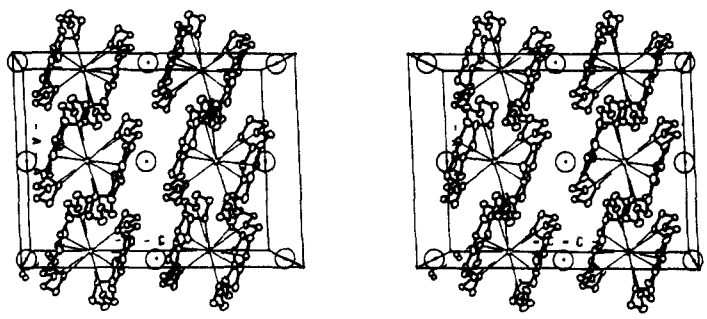

Figure 1. ORTEP stereo packing diagram of $Cs^+(18C6)_2 \cdot e^-$. The anionic hole centers are indicated by the symbol ⊙.

Figure 2. ORTEP stereodiagram of the anionic hole and surrounding atoms in $Cs^+(18C6)_2 \cdot e^-$ viewed along the b axis.

0002-7863/86/1508-3534$01.50/0